

# Feedback-Based Quantum Control for Safe and Synergistic Drug Combination Design

Mai Nguyen Phuong Nhi,<sup>1,2</sup> Lan Nguyen Tran,<sup>1,2</sup> and Le Bin Ho<sup>3,4</sup>

<sup>1</sup> University of Science, Vietnam National University, Ho Chi Minh City 700000, Vietnam

<sup>2</sup> Vietnam National University, Ho Chi Minh City 700000, Vietnam

<sup>3</sup> Frontier Research Institute for Interdisciplinary Sciences, Tohoku University, Sendai 980-8578, Japan

<sup>4</sup> Department of Applied Physics, Graduate School of Engineering, Tohoku University, Sendai 980-8579, Japan

(Dated: January 27, 2026)

Drug-drug interactions (DDIs) strongly affect the safety and efficacy of combination therapies. Despite the availability of large DDI databases, selecting optimal multi-drug combinations that balance safety, therapeutic benefit, and regimen size remains a challenging combinatorial optimization problem. Here, we present a quantum-control-based framework for DDI-aware drug combination optimization, in which known harmful and synergistic interactions are encoded into Ising Hamiltonians as penalties and rewards, respectively. The optimization is performed using the feedback-based quantum algorithm FALQON, a gradient-free variational approach. We study two clinically motivated tasks: the Maximum Safe Subset problem and the Synergy-Constrained Optimization problem. Numerical simulations using interaction data from Drugs.com and SYNERGxDB demonstrate efficient convergence and high-quality solutions for clinically relevant drug sets, including COVID-19 case studies.

## I. INTRODUCTION

Drug-drug interactions (DDIs) are a common cause of harmful side effects, treatment failure, and hospital admission in modern medicine [1–4]. These problems become more serious as patients are increasingly treated with multiple drugs (polypharmacy) at the same time, for example in cancer therapy, long-term treatment of chronic diseases, or infectious diseases [5–8]. As more drugs are combined, the number of possible interactions grows very quickly, and even one dangerous combination can put a patient at serious risk [5, 7]. Well-known examples include severe bleeding caused by certain combinations of blood thinners [9, 10], muscle damage [11, 12], and kidney failure [13] that can occur when some cholesterol-lowering drugs are taken together with specific antibiotics.

On the other hand, many effective treatments intentionally rely on positive drug interactions [14–17]. Combination therapies are widely used in HIV treatment [16, 18], cancer chemotherapy [15, 19], and antibiotic regimens [20], where multiple drugs work together to improve effectiveness or prevent resistance. During the COVID-19 pandemic, several treatment strategies explored combinations of antiviral, anti-inflammatory, and supportive drugs, where both beneficial synergy and harmful interactions had to be carefully considered [16, 21–23].

While substantial effort has been devoted to predicting DDIs and curating interaction databases [24–26], an equally important downstream challenge remains: *selecting safe and effective multi-drug regimens given existing DDI knowledge*. In clinical practice, interaction data are typically treated as fixed input, and the main difficulty lies in exploring the rapidly growing space of possible drug combinations while simultaneously avoiding harmful interactions and leveraging therapeutic synergy. This combinatorial complexity, together with the high cost of

experimental and clinical validation, motivates the development of advanced optimization approaches, including quantum-assisted and quantum-inspired methods, for systematic drug combination design.

From a computational perspective, selecting an optimal subset of drugs from a library of size  $n$  can be naturally formulated as a graph problem, where nodes represent drugs and edges encode harmful or synergistic interactions [24–30]. Finding the largest harm-free combination corresponds to a maximum independent-set problem on the harmful subgraph, while identifying a high-synergy, size-constrained combination with toxicity penalties leads to more general quadratic unconstrained binary optimization (QUBO) formulations [31]. These problems are NP-hard and quickly become intractable for classical exhaustive search as  $n$  grows, even when heuristic or approximate methods are employed [32].

Quantum optimization algorithms provide a potential route to addressing such combinatorial explosions. The quantum approximate optimization algorithm (QAOA) has emerged as a widely studied framework for encoding discrete optimization problems into parameterized quantum circuits [33]. However, QAOA suffers from several limitations that are particularly severe on noisy intermediate-scale quantum (NISQ) devices: circuit depth grows with the number of layers, classical parameter optimization can be slow and prone to barren plateaus [34], and constrained problems often require delicate tuning of penalty terms. These challenges motivate the exploration of alternative quantum strategies that can handle complex constraint structures without incurring large classical overhead.

In this work, we introduce a quantum-control-based framework for *DDI-aware drug combination optimization* based on the feedback-based quantum control algorithm (FALQON) [35] and its imaginary-time extension (ITE-FALQON) [36]. FALQON eliminates the classical outer-loop optimization of QAOA by employing an intrinsic

feedback law that updates a single control field using instantaneous quantum expectation values. The system evolves under a time-dependent Hamiltonian of the form  $\mathcal{H}(t) = \mathcal{H}_p + \beta(t)\mathcal{H}_d$ , where  $\mathcal{H}_p$  encodes the DDI-aware objective and  $\mathcal{H}_d$  is a simple driver Hamiltonian. This feedback mechanism enforces a monotonic decrease of the objective energy, effectively implementing quantum gradient descent without explicit gradient evaluation or multi-parameter tuning.

Within this framework, we formulate two complementary DDI optimization tasks. The first is the *Maximum Safe Subset* (MSS) problem, which seeks the largest set of drugs that contains no harmful interactions and can be mapped to an Ising Hamiltonian with purely penalizing couplings. The second is the *Synergy-Constrained Optimization* (SCO) problem, which augments the MSS model by incorporating synergy rewards and a cardinality constraint, thereby capturing the trade-off between efficacy, toxicity, and regimen size. Both objectives are encoded as Ising Hamiltonians derived from clinically documented interaction data obtained from sources such as Drugs.com and SYNERGxDB, with interaction strengths normalized to reflect relative severity or synergy.

We demonstrate our approach on a six-drug network consisting of Ritonavir, Everolimus, Cabazitaxel, Metformin, Erlotinib, and Topotecan. These drugs span distinct pharmacological classes and exhibit a complex structure of both harmful and synergistic interactions. We show that ITE-FALQON rapidly converges to low-energy configurations of the MSS and SCO Hamiltonians, outperforming standard FALQON, and reliably identifies clinically meaningful drug subsets. We further apply the method to a COVID-19 case study involving nine drug candidates. Our results highlight the advantages of feedback-based quantum control for constrained biomedical optimization problems. More broadly, they suggest that FALQON and related control-based algorithms offer a promising route toward quantum-assisted decision support for drug combination design.

The paper is organized as follows. In Sec. II, we introduce the theoretical framework and define two complementary DDI optimization tasks: MSS and SCO. Section III provides a brief overview of the optimization methods, including FALQON and ITE-FALQON. Numerical implementation details and benchmark results are presented in Sec. IV. In Sec. V, we apply our approach to a COVID-19 case study. Finally, Secs. VI and VII are devoted to discussion and conclusions, respectively.

## II. THEORETICAL FRAMEWORK

In this section, we introduce the mathematical framework used to encode DDI data into an Ising Hamiltonian suitable for quantum optimization. We begin with a drug library

$$\mathcal{D} = \{d_1, d_2, \dots, d_n\}, \quad (1)$$

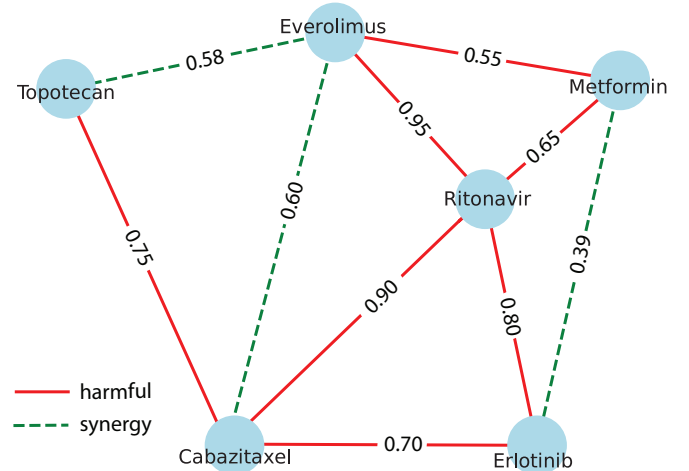


FIG. 1. Interaction graph of the six-drug network. Nodes represent individual drugs, while edges indicate pairwise interactions. Red edges denote harmful interactions and green edges denote synergistic interactions. Numbers on the edges indicate the corresponding interaction weights.

where each drug  $d_i$  is represented by a binary decision variable  $x_i \in \{0, 1\}$ , with  $x_i = 1$  indicating that drug  $i$  is included in the proposed combination and  $x_i = 0$  otherwise. A candidate multi-drug combination is represented by the bitstring  $\mathbf{x} = (x_1, \dots, x_n)$ .

The DDI data are encoded in a weighted graph

$$G = (\mathcal{D}, \mathcal{E}_{\text{harm}} \cup \mathcal{E}_{\text{syn}}), \quad (2)$$

where vertices represent drugs and edges denote either harmful (belong to a subset  $\mathcal{E}_{\text{harm}}$ ) or synergistic (belong to a subset  $\mathcal{E}_{\text{syn}}$ ) interactions. Each edge  $(i, j)$  is assigned a weight that quantifies the clinical severity of a harmful interaction or the strength of a synergistic effect. These values are extracted from established pharmacological resources, including Drugs.com and SYNERGxDB.ca and normalized to the interval  $[0, 1]$ . In Fig. 1, we illustrate a graph of 6 drugs as summarized in Tab. I.

TABLE I. DDI dataset used in the simulation (weights inferred from clinical severity).

drug <sub>i</sub>	drug <sub>j</sub>	kind	weight $w_{ij}^{\text{kind}}$
Ritonavir	Everolimus	harm	0.95
Ritonavir	Cabazitaxel	harm	0.90
Metformin	Ritonavir	harm	0.65
Metformin	Everolimus	harm	0.55
Ritonavir	Erlotinib	harm	0.80
Topotecan	Cabazitaxel	harm	0.75
Erlotinib	Cabazitaxel	harm	0.70
Everolimus	Cabazitaxel	synergy	0.60
Everolimus	Topotecan	synergy	0.58
Erlotinib	Metformin	synergy	0.39

The goal of the optimization is to choose a group of drugs that is safe to use together and, when possible,

provides useful therapeutic benefits. To do this, we build an objective function that accounts for harmful interactions, possible synergy between drugs, and the preferred number of drugs in the combination. We introduce two models below that describe how these requirements are encoded.

### A. Maximum Safe Subset (MSS)

The first task is the *Maximum Safe Subset* (MSS) problem. Here, the objective is to choose the largest possible set of drugs that contains no harmful interactions. In other words, we seek the largest drug combination in which all drugs can be safely used together.

To encode this objective, we assign a reward for selecting each drug and impose a penalty for selecting any harmful pair. The loss function is

$$\mathcal{L}_{\text{MSS}}(\mathbf{x}) = - \sum_{i=1}^n x_i + \alpha \sum_{(i,j) \in \mathcal{E}_{\text{harm}}} w_{ij}^{\text{harm}} x_i x_j, \quad (3)$$

where  $\alpha > 0$  is a penalty coefficient controlling the severity of constraint enforcement and  $w_{ij}^{\text{harm}}$  are harmful weights. The first term encourages selecting as many drugs as possible, while the second term penalizes the inclusion of any harmful pair. If  $\alpha$  is sufficiently large, the optimal solution will exclude all harmful pairs entirely.

To convert Eq. (3) into an Ising Hamiltonian, we map

$$x_i = \frac{1 - z_i}{2},$$

where  $z_i \in \{-1, +1\}$  are Pauli-Z eigenvalues. Substituting this relation into Eq. (3) yields an Ising Hamiltonian

$$\mathcal{H}_{\text{MSS}} = c^{\text{MSS}} + \sum_i h_i^{\text{MSS}} Z_i + \sum_{i < j} J_{ij}^{\text{MSS}} Z_i Z_j, \quad (4)$$

where  $Z_i$  is the Pauli-Z operator acting on qubit  $i$ , and the coefficients determined explicitly by

$$c^{\text{MSS}} = -\frac{n}{2} + \frac{\alpha}{4} \sum_{(i,j) \in \mathcal{E}_{\text{harm}}} w_{ij}^{\text{harm}}, \quad (5)$$

$$h_i^{\text{MSS}} = \frac{1}{2} - \frac{\alpha}{4} \sum_{(i,j) \in \mathcal{E}_{\text{harm}}} w_{ij}^{\text{harm}}, \quad (6)$$

$$J_{ij}^{\text{MSS}} = \frac{\alpha}{4} w_{ij}^{\text{harm}}. \quad (7)$$

Thus, harmful interactions generate positive Ising couplings  $J_{ij}^{\text{MSS}} > 0$ , raising the energy of configurations where both  $z_i = z_j = -1$  (i.e.,  $x_i = x_j = 1$ ). The ground state of this Hamiltonian corresponds exactly to the largest safe drug subset.

### B. Synergy-Constrained Optimization (SCO)

While the MSS formulation focuses exclusively on safety by eliminating harmful drug pairs, many therapeutic applications demand a more nuanced balance between

efficacy and toxicity [37]. In clinical practice, desirable drug combinations simultaneously exploit beneficial synergy, avoid adverse interactions, and meet a prescribed therapeutic size. To accommodate these competing requirements, we introduce the *Synergy-Constrained Optimization* (SCO) model, which extends the MSS formalism by incorporating synergistic rewards and a cardinality constraint.

In SCO, the objective function contains three contributions. First, synergistic interactions decrease the loss, favoring the co-selection of pharmacologically compatible drug pairs. Second, harmful interactions increase the loss through a toxicity penalty weighted by a parameter  $\gamma$ , which allows us to modulate the strictness of harm suppression. Third, a quadratic regularization term enforces a target combination size  $K$ , ensuring that the resulting drug set satisfies application-specific design criteria. These considerations lead to the loss function

$$\begin{aligned} \mathcal{L}_{\text{SCO}}(\mathbf{x}) = & - \sum_{(i,j) \in \mathcal{E}_{\text{syn}}} w_{ij}^{\text{syn}} x_i x_j + \gamma \sum_{(i,j) \in \mathcal{E}_{\text{harm}}} w_{ij}^{\text{harm}} x_i x_j \\ & + \mu \left( \sum_{i=1}^n x_i - K \right)^2, \end{aligned} \quad (8)$$

where  $\gamma$  tunes the harmful penalty,  $\mu$  controls the strength of the size constraint, and  $K$  denotes the desired number of selected drugs. The quadratic term introduces both local fields and effective all-to-all couplings once expanded, reflecting the global nature of the cardinality requirement.

Substituting the standard Ising mapping  $x_i = (1 - z_i)/2$  into Eq. (8) yields an Ising Hamiltonian as

$$\mathcal{H}_{\text{SCO}} = c^{\text{SCO}} + \sum_i h_i^{\text{SCO}} Z_i + \sum_{i < j} J_{ij}^{\text{SCO}} Z_i Z_j, \quad (9)$$

where

$$\begin{aligned} c^{\text{SCO}} = & -\frac{1}{4} \sum_{(i,j) \in \mathcal{E}_{\text{syn}}} w_{ij}^{\text{syn}} \\ & + \frac{\gamma}{4} \sum_{(i,j) \in \mathcal{E}_{\text{harm}}} w_{ij}^{\text{harm}} + \mu \left( \frac{n}{2} - K \right)^2 + \mu \frac{n}{4}, \end{aligned} \quad (10)$$

$$h_i^{\text{SCO}} = \frac{1}{4} \sum_{j \in \mathcal{E}_{\text{syn}}} w_{ij}^{\text{syn}} - \frac{\gamma}{4} \sum_{j \in \mathcal{E}_{\text{harm}}} w_{ij}^{\text{harm}} - \mu \left( \frac{n}{2} - K \right), \quad (11)$$

$$J_{ij}^{\text{SCO}} = -\frac{1}{4} w_{ij}^{\text{syn}} + \frac{\gamma}{4} w_{ij}^{\text{harm}} + \frac{\mu}{2}. \quad (12)$$

The sign and magnitude of the couplings have clear pharmacological meaning: synergistic pairs generate negative couplings, which energetically favor their co-selection, harmful pairs generate positive couplings, which penalize configurations containing both drugs, and the cardinality term induces global correlations that steer the system toward the prescribed combination size. Consequently, the ground state of  $\mathcal{H}_{\text{SCO}}$  encodes the optimal clinically constrained drug set, simultaneously balancing efficacy, safety, and size.

### III. QUANTUM OPTIMIZATION METHODS

To find the ground energy and ground state (bitstring solution) of  $\mathcal{H}_{\text{MSS}}$  and  $\mathcal{H}_{\text{SCO}}$ , we apply the feedback-based quantum control algorithm (FALQON) [35] and a recent developed method imaginary-time evolution enhanced FALQON (ITE-FALQON) [36].

#### A. FALQON

Unlike hybrid variational methods such as QAOA, which rely on repeated circuit executions combined with classical parameter optimization, FALQON determines its control parameters directly from the quantum dynamics. This eliminates the need for classical training and makes the method particularly effective for constrained combinatorial problems with highly nonconvex energy landscapes.

The quantum state evolves under a time-dependent Hamiltonian

$$\mathcal{H}(t) = \mathcal{H}_p + \beta(t)\mathcal{H}_d, \quad (13)$$

where  $\mathcal{H}_p$  is the problem Hamiltonian, i.e.,  $\mathcal{H}_{\text{MSS}}, \mathcal{H}_{\text{SCO}}$ , and  $\mathcal{H}_d = \sum_i X_i$  is a driver Hamiltonian that induces transitions between computational basis states. All pharmacological information is contained in  $\mathcal{H}_p$ ; therefore, its ground state corresponds to the optimal drug combination.

The feedback mechanism adjusts the control field  $\beta(t) = -i\langle\psi(t)|[\mathcal{H}_d, \mathcal{H}_p]|\psi(t)\rangle$  such that the expectation value

$$C(t) = \langle\psi(t)|\mathcal{H}_p|\psi(t)\rangle, \quad (14)$$

decreases monotonically during the evolution. The update rule is determined by the instantaneous commutator between  $\mathcal{H}_d$  and  $\mathcal{H}_p$ , which identifies the direction of energy descent. In this way, FALQON implements a quantum analogue of gradient descent without explicitly computing gradients or optimizing multiple variational parameters.

In practice, the evolution is discretized into a sequence of alternating applications of  $\mathcal{H}_p$  and  $\mathcal{H}_d$ , with the control field updated at each step through the feedback rule. The circuit depth therefore grows linearly with the number of time steps, making the algorithm robust to noise and suitable for near-term quantum hardware. In the DDI setting, this dynamical process naturally suppresses unsafe drug combinations while amplifying configurations that satisfy the MSS or SCO objectives.

#### B. ITE-FALQON

To further accelerate convergence toward the ground state and suppress residual excited-state components, we

consider an extension of FALQON based on imaginary-time evolution or ITE-FALQON [36]. In imaginary time, the state propagation is governed by the non-unitary transformation

$$|\psi(\tau + \Delta\tau)\rangle \propto e^{-\Delta\tau\mathcal{H}_p}|\psi(\tau)\rangle,$$

which acts as an energy filter.

By expanding the state in the energy eigenbasis of  $\mathcal{H}_p$ , imaginary-time evolution exponentially suppresses higher-energy components relative to the ground state. As the imaginary time  $\tau$  increases, the state is progressively projected onto the lowest-energy subspace, thereby enhancing ground-state fidelity.

Within the ITE-FALQON framework, this energy-filtering mechanism is combined with the feedback-controlled dynamics of FALQON. The resulting evolution guides the system more directly toward the true ground state of the  $\mathcal{H}_{\text{MSS}}$  and  $\mathcal{H}_{\text{SCO}}$ , improving convergence speed and stability, particularly in cases where the energy spectrum is dense or near-degenerate [36].

## IV. IMPLEMENTATION DETAILS

#### A. Model setup

We construct a six-drug interaction network from clinically documented data, as shown in Fig. 1 and Tab. I. The drug set includes Ritonavir, Everolimus, Cabazitaxel, Metformin, Erlotinib, and Topotecan, which covers antiviral, oncological, and metabolic therapies and exhibits a range of harmful and synergistic interactions. This combination provides a compact yet representative testbed for DDI optimization. The interaction graph contains weighted harmful edges, which introduce energetic penalties, and synergistic edges, which lower the energy of favorable combinations. This graph fully determines the Ising Hamiltonians used in the FALQON and ITE-FALQON simulations.

All numerical simulations are performed using the Qiskit statevector backend. Each drug is encoded by a single qubit, and the corresponding Ising Hamiltonians are constructed from standard Pauli- $Z$  and  $ZZ$  operators according to  $\mathcal{H}_{\text{MSS}}$  and  $\mathcal{H}_{\text{SCO}}$ . The mixer Hamiltonian consists of a sum of single-qubit Pauli- $X$  operators.

The quantum evolution is discretized into  $T$  time steps. At each step, the control field  $\beta(t)$  is updated using the FALQON feedback rule. For ITE-FALQON, an imaginary-time evolution step is applied after every two FALQON updates. The imaginary-time step size  $\Delta\tau$  is chosen separately for each model to account for differences in energy scales. For the MSS problem, we use  $\Delta\tau = 0.1$ , while the SCO problem requires a smaller step size,  $\Delta\tau = 0.01$ , to ensure numerical stability. This smaller  $\Delta\tau$  is necessary because the SCO Hamiltonian includes a quadratic cardinality constraint,  $\mu(\sum_i x_i - K)^2$ , which leads to larger energy eigenvalues and all-to-all couplings.

After the final evolution, measurements yield a probability distribution over all bitstrings, where the most probable low-energy states correspond to candidate drug combinations satisfying the MSS or SCO criteria.

## B. MSS Results

We first investigate the MSS problem by applying FALQON and ITE-FALQON to the Hamiltonian  $\mathcal{H}_{\text{MSS}}$ . Figure 2 shows the time evolution of the energy  $E(t) = \langle \psi(t) | \mathcal{H}_{\text{MSS}} | \psi(t) \rangle$  for several values of the penalty parameter  $\alpha$ , which controls the energetic cost of violating harmful-interaction constraints.

For all values of  $\alpha$ , FALQON drives the system toward the correct low-energy subspace and reliably identifies the optimal safe configuration. However, because the evolution is purely unitary, the final energy saturates slightly above the exact ground-state value. This residual offset reflects the presence of excited-state components that are not explicitly suppressed under unitary dynamics.

In contrast, ITE-FALQON converges rapidly and reaches the exact ground-state energy for all tested values of  $\alpha$ . The imaginary-time component effectively filters out higher-energy contributions, leading to a sharp projection onto the ground state and significantly faster convergence.

The role of the penalty parameter  $\alpha$  is also evident. Increasing  $\alpha$  amplifies the energetic separation between valid (harm-free) configurations and invalid ones, thereby enlarging the spectral gap of  $\mathcal{H}_{\text{MSS}}$ . This enhanced separation accelerates convergence in both algorithms, with the effect being particularly pronounced for ITE-FALQON, which exploits the widened gap through exponential suppression of excited states.

These results demonstrate that while FALQON is sufficient to identify the correct MSS solution, the inclusion of imaginary-time evolution substantially improves convergence speed and accuracy by enforcing explicit energy filtering.

Figure 3(a) shows the measurement probabilities after the FALQON evolution. As expected for the MSS objective, significant probability accumulates only on configurations that contain no harmful interactions. The distribution is strongly dominated by two bitstrings, 111000 and 110100, with probabilities of approximately 0.49 and 0.46, respectively. All remaining bitstrings appear with probabilities below  $2 \times 10^{-2}$ , indicating that unsafe configurations are effectively suppressed.

Importantly, the identity of these dominant bitstrings is independent of the specific value of the penalty coefficient  $\alpha$ , provided that  $\alpha$  is large enough to energetically separate unsafe states. Increasing  $\alpha$  therefore does not change which configurations are optimal, but instead reinforces the energetic separation between feasible and infeasible subsets. In Fig. 3, we use  $\alpha = 5$ . The coexistence of two dominant solutions reflects the fact that the MSS problem admits multiple maximum safe subsets

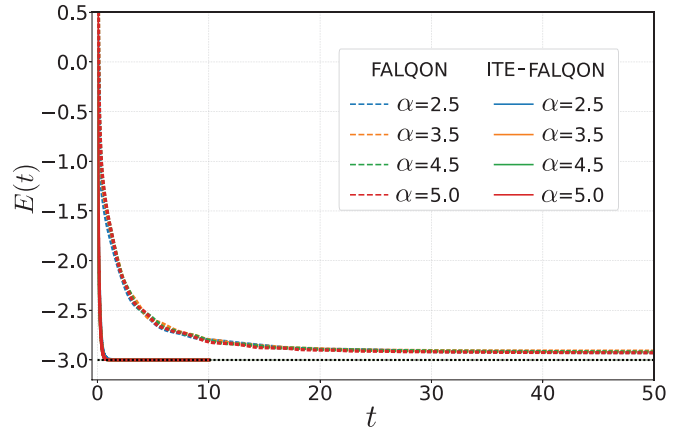


FIG. 2. Energy evolution obtained using FALQON and ITE-FALQON for different penalty coefficients  $\alpha$ . While FALQON reliably identifies the correct optimal bitstring, its final energy remains slightly above the exact ground-state energy due to the purely unitary nature of the dynamics, which does not explicitly suppress excited-state components. In contrast, ITE-FALQON rapidly reaches the ground-state energy by effectively filtering out higher-energy contributions through imaginary-time evolution. This comparison highlights the complementary roles of feedback-based control and non-unitary energy filtering in accelerating convergence.

with equal cardinality and nearly degenerate energies.

Figure 3(b) shows the corresponding results obtained using ITE-FALQON. In this case, the probability distribution becomes even more sharply concentrated: essentially all probability mass collapses onto the same two bitstrings, 111000 and 110100, with nearly equal weights. All other configurations are suppressed to negligible probabilities. This behavior is a direct consequence of the imaginary-time component, which exponentially filters out excited-state contributions and projects the system more efficiently onto the ground-state subspace [36].

The network visualizations in Fig. 3(b) illustrate the drug subsets represented by these two bitstrings. Shaded nodes indicate the selected drugs. Both configurations exclude all major harmful interactions, confirming that they correspond to valid maximum safe subsets. The near-equal probabilities and energies of the two solutions highlight the intrinsic degeneracy of the MSS problem and demonstrate that ITE-FALQON faithfully recovers the complete set of optimal safe regimens.

## C. SCO Results

We now turn to the SCO problem, which extends the MSS formulation by incorporating both synergistic rewards and an explicit cardinality constraint. The objective is to identify drug combinations of fixed size  $K$  that maximize therapeutic synergy while suppressing harmful interactions. In the results shown here, we apply the

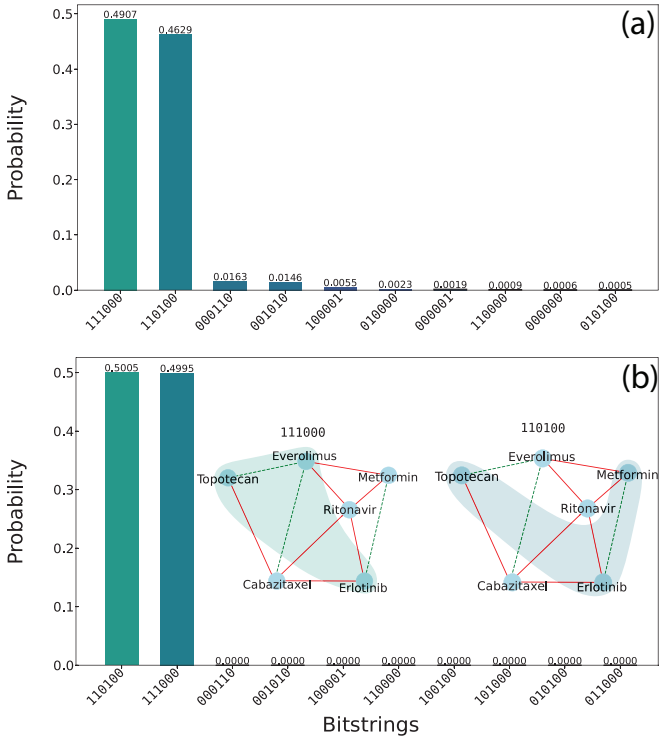


FIG. 3. Final probability distributions and dominant MSS solutions. (a) FALQON concentrates probability on two harm-free bitstrings, 111000 and 110100, while suppressing unsafe configurations. (b) ITE-FALQON further sharpens this distribution, projecting almost entirely onto the same two degenerate MSS solutions. The shaded graphs depict the corresponding drug subsets.

ITE-FALQON algorithm and compare two target sizes,  $K = 3$  and  $K = 4$ , why we fix  $\gamma = 2.5$  and  $\mu = 5$ .

Figure 4 summarizes the SCO performance. Fig. 4(a) shows the time evolution of the energy  $E(t) = \langle \psi(t) | \mathcal{H}_{\text{SCO}} | \psi(t) \rangle$ . In both cases of  $K$ , the energy rapidly decreases and stabilizes within a short optimization time, indicating efficient suppression of excited-state contributions. The difference in the final energy reflects the imposed cardinality constraint: increasing  $K$  shifts the optimal energy upward due to the larger number of selected drugs and the associated interaction terms.

Figure 4 (b, c) show the final measurement probability distributions for  $K = 3$  and  $K = 4$ , respectively. In both cases, the dynamics concentrate almost entirely on a single bitstring, demonstrating that the optimization uniquely selects a dominant optimal solution. The corresponding interaction graphs highlight that the selected drug subsets simultaneously satisfy the size constraint, avoid harmful internal interactions, and preferentially include synergistic pairs.

These results show that the SCO formulation reliably extracts clinically interpretable drug combinations. The dominant bitstrings correspond to subsets that are internally consistent with known DDI structure, while the changes observed between  $K = 3$  and  $K = 4$  directly re-

flect the underlying pharmacological constraints encoded in the interaction network.

## V. COVID-19 CASE STUDY

During the early stages of the COVID-19 pandemic, many drugs were tested in clinical trials to find effective combinations against SARS-CoV-2. Because a large number of possible drug combinations were proposed, identifying the best subsets quickly became a challenging combinatorial optimization problem. Motivated by this challenge, we apply the ITE-FALQON method to a panel of nine drugs to examine whether clinically effective drug subsets can be recovered by minimizing a Hamiltonian constructed from pairwise drug interactions.

The drugs are grouped into three functional classes: viral replication inhibitors, entry and post-translational inhibitors, and immune response regulators. The diversity of these mechanisms leads to both cooperative and conflicting interactions, creating a complex optimization landscape that is well suited for benchmarking the ITE-FALQON framework. Table II summarizes the pharmacological mechanisms and abbreviations used for each drug in this study.

Pairwise synergy and harmful interaction weights were obtained from the Liverpool COVID-19 Drug Interaction database and supporting pharmacological studies. These weights were normalized to the range  $[0, 1]$ , where strongly complementary antiviral pairs were assigned high synergy, and harmful interactions were identified based on reported adverse effects (see Table III). For example, Remdesivir and Ribavirin show synergistic antiviral activity and are therefore assigned a high synergy weight, whereas the combination of Remdesivir and Hydroxychloroquine is known to reduce antiviral efficacy and is classified as harmful. The interaction graph is shown in Fig. 5.

This procedure encodes the known drug interaction structure directly into the Hamiltonian while remaining robust to uncertainties in quantitative interaction strengths. Importantly, the optimization relies only on pairwise interactions, with no higher-order terms or training data introduced.

### A. MSS Results

When applying the MSS Hamiltonian to this drug set, we observe a clear dependence of the low-energy solutions on the penalty factor  $\alpha$ . For relatively small values of  $\alpha$  (e.g.,  $\alpha=2.5$ ), the optimal solutions is  $\{\text{RDV, RBV, PAX, NTZ, MOV, FPV, DEX}\}$ , which still contains harmful terms, such as the PAX-DEX pair because the energy of adding a new drug can outweigh the penalty imposed by a harmful interaction. As a result, the algorithm accepts a trade-off between maximizing the subset size and tolerating limited safety violations.

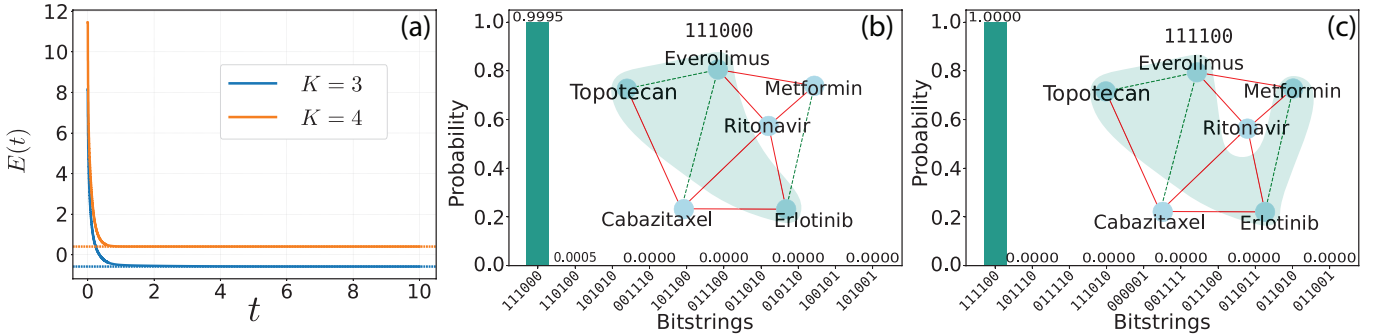


FIG. 4. SCO results obtained using ITE-FALQON. (a) Energy convergence for target cardinalities  $K = 3$  and  $K = 4$ . (b, c) Final measurement probability distributions and corresponding interaction graphs for  $K = 3$  and  $K = 4$ , respectively. In both cases, the dynamics concentrate almost entirely on a single dominant bitstring, indicating a unique optimal drug combination. The inset graphs visualize the selected subsets and their internal interactions, illustrating the balance between synergistic benefit and interaction risk as the cardinality constraint is increased.

TABLE II. Classification and mechanism of action for 9 drugs included in the COVID-19 repurposing case study. Abbreviations are used in the interaction graphs and Hamiltonian encoding.

Drug Name	Abbreviation	Primary Mechanism / Pharmacological Class
<i>Viral Replication Inhibitors (Antivirals)</i>		
Remdesivir	RDV	Nucleoside analog; RdRp inhibitor [38, 39]
Molnupiravir	MOV	Ribonucleoside analog; induces lethal mutagenesis [38, 39]
Favipiravir	FPV	Purine analog; selective RdRp inhibitor [38, 39]
Ribavirin	RBV	Guanosine analog; interferes with RNA synthesis [38, 39]
Nirmatrelvir/Ritonavir	PAX	SARS-CoV-2 main protease (Mpro/3CLpro) inhibitor [38, 39]
Lopinavir/Ritonavir	LPV	HIV protease inhibitor (repurposed) [38, 39]
<i>Entry and Post-Translational Inhibitors</i>		
Nitazoxanide	NTZ	Broad-spectrum; inhibits viral entry/assembly [38, 39]
Hydroxychloroquine	HCQ	Antimalarial; modulates endosomal pH [38, 39]
<i>Immune Response Regulation</i>		
Dexamethasone	DEX	Corticosteroid; anti-inflammatory/immunomodulator [38, 39]

As the penalty factor is increased, the tendency of en-

TABLE III. COVID-19 DDI dataset (weights from literature).

drug <sub>i</sub>	drug <sub>j</sub>	kind	weight $w_{ij}^{\text{kind}}$
RBV	RDV	synergy	0.95
MOV	PAX	synergy	0.90
MOV	RDV	synergy	0.80
MOV	RBV	synergy	0.60
PAX	RDV	synergy	0.55
FPV	MOV	synergy	0.95
NTZ	RDV	synergy	0.85
HCQ	RDV	harm	0.95
HCQ	PAX	harm	0.40
LPV	PAX	harm	0.75
LPV	RDV	harm	0.40
DEX	HCQ	harm	0.75
DEX	PAX	harm	0.30
FPV	LPV	harm	0.70

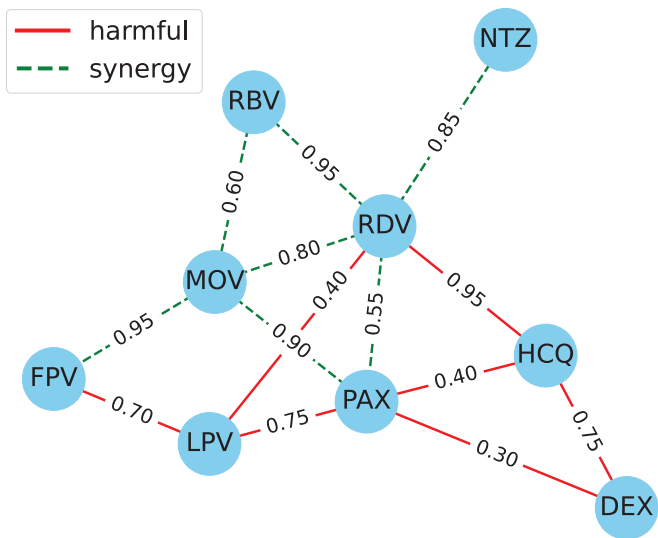


FIG. 5. Interaction graph of the 9-drug network.

ergy landscape starts to change: all dominant low-energy configurations systematically exclude harmful pairs. For example, with  $\alpha = 5$ , we get  $\{\text{RDV}, \text{RBV}, \text{NTZ}, \text{MOV}, \text{FPV}, \text{DEX}\}$ , which no harmful interaction at all. This

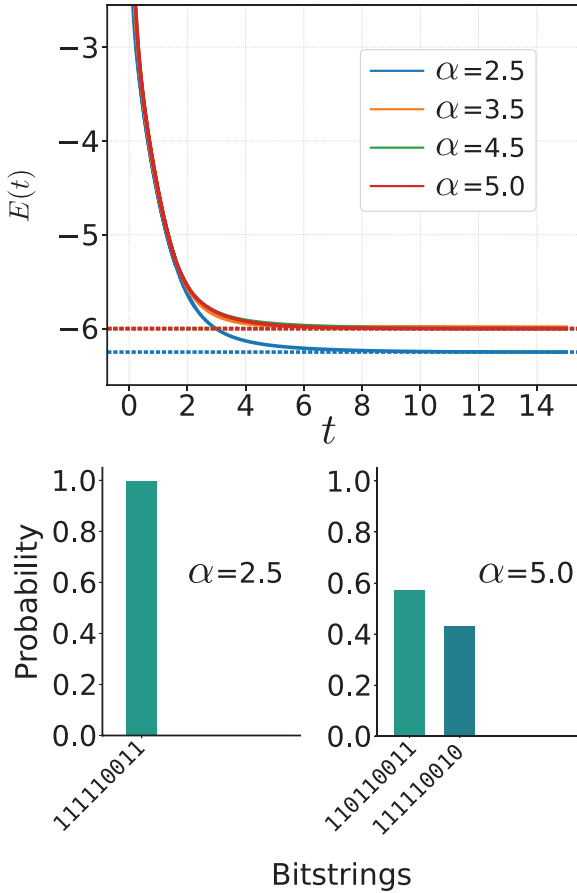


FIG. 6. (upper) Energy evolution obtained from the ITE-FALQON for different penalty coefficients  $\alpha$ . (lower) Final probability distributions and dominant MSS solutions. (left) For relatively small values of  $\alpha$  (e.g.,  $\alpha=2.5$ ), the optimal solutions is  $\{\text{RDV, RBV, PAX, NTZ, MOV, FPV, DEX}\}$ , which still contains harmful terms. (right) For  $\alpha=5$ , we get  $\{\text{RDV, RBV, NTZ, MOV, FPV, DEX}\}$ , which no harmful interaction at all.

behavior is consistent with the MSS objective, which identifies the largest subset of drugs that remains compliant with safety constraints. In conclusion, penalty factor  $\alpha$  plays an important role in reflecting different levels of clinical risk tolerance, and larger  $\alpha$  is better.

## B. SCO Results

We next consider the SCO setting by imposing a specific constraint on the selected subset, fixing the number of drugs to  $K = 3$ . Under this constraint, we obtain the most dominant bitstring corresponding to the drug triples  $\{\text{RDV, RBV, MOV}\}$ . Moreover, in vitro and animal model studies have shown that both combinations can enhance antiviral efficacy including synergistic suppression of SARS-CoV-2 replication. Compared to the MSS formulation, which favors selecting as many mutually non-harmful drugs as possible, the SCO formulation

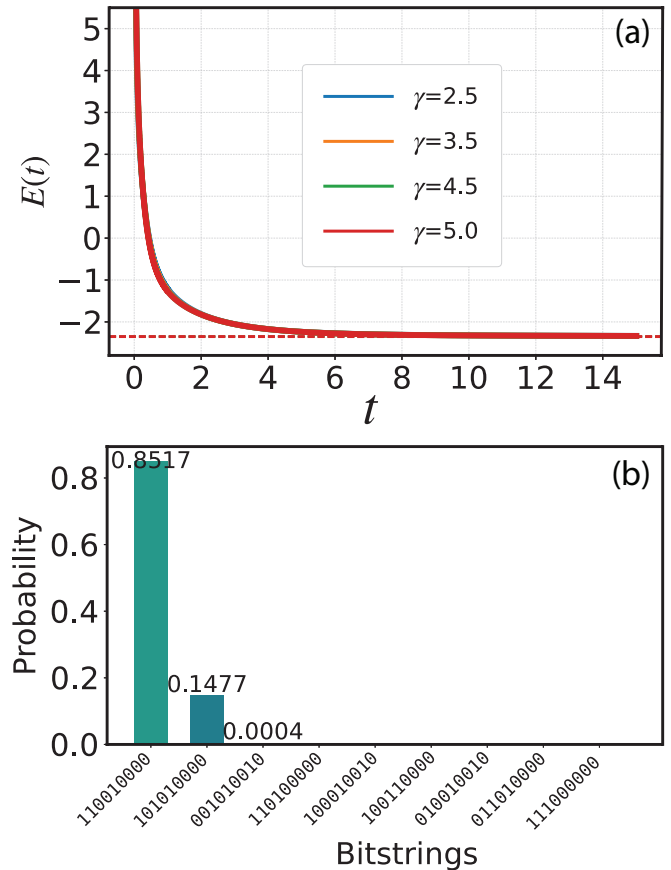


FIG. 7. (a) Energy evolution obtained from ITE-FALQON for different penalty coefficients  $\gamma$ . (b) Under this constraint, we obtain the most dominant bitstring corresponding to the drug triples  $\{\text{RDV, RBV, MOV}\}$ .

is more aligned with clinical practice by restricting the size of the optimal drug subset. In the context of actual COVID-19 treatment, increasing the number of co-administered drugs may increase the risk of toxicity due to higher-order polypharmacy effects, even in the absence of pairwise conflicts. This case study serves as a proof-of-principle that ITE-FALQON framework can recover clinically meaningful drug combinations within a large combinatorial search space using only pairwise interaction information encoded in a physical Hamiltonian.

## VI. DISCUSSION

The present results show that FALQON and ITE-FALQON can reliably identify safe or synergistic subsets in small DDI networks, and the structure of real pharmacological data suggests that the method can scale beyond the six-drug examples studied here. Large clinical DDI databases such as DrugBank or SYNERGxDB contain hundreds of drugs, but the corresponding interaction graphs are highly sparse: only a small fraction of drug pairs exhibit clinically documented interactions. This

sparsity substantially reduces the number of nonzero couplings in the Ising Hamiltonian and therefore mitigates the growth of circuit complexity as the number of drugs increases.

A second feature of real DDI networks is their modularity. Harmful or synergistic interactions tend to cluster within drug classes, allowing the Hamiltonian to be organized into blocks that can be encoded efficiently. Together, sparsity and modularity imply that Hamiltonians derived from realistic DDI datasets remain tractable for statevector simulations and for near-term quantum hardware in the 50-100 qubit range, provided that appropriate preprocessing steps are applied.

From an algorithmic perspective, FALQON and its extend version offer clear advantages over variational approaches such as QAOA. Because the control field is updated through a closed-loop quantum expectation value rather than a classical optimization routine, FALQON avoids barren plateaus and does not require deep, parameter-heavy circuits. Its depth grows only linearly with the number of time steps, making the method robust to noise and well suited to constrained optimization problems like MSS and SCO, where large penalties induce steep energy landscapes.

These properties suggest that FALQON provides a promising route toward quantum-assisted analysis of clinically relevant DDI networks. Embedding real-world synergy and toxicity scores directly into the Hamiltonian is straightforward, and future work will focus on scaling to larger datasets and incorporating richer pharmacokinetic constraints.

## VII. CONCLUSION

We have presented a quantum control-based framework for DDI-aware drug combination optimization using the FALQON and ITE-FALQON algorithms. By encoding clinically documented drug-drug interaction data into Ising Hamiltonians, our approach efficiently identifies safe and synergistic multi-drug combinations with reduced computational overhead. These results highlight the potential of feedback-based quantum control algorithms as practical tools for constrained combinatorial optimization in biomedical decision support and rational multi-drug therapy design.

## ACKNOWLEDGMENTS

This paper is supported by JSPS KAKENHI Grant Number 23K13025, and the Tohoku Initiative for Fostering Global Researchers for Interdisciplinary Sciences (TI-FRIS) of MEXT's Strategic Professional Development Program for Young Researchers. L.N.T is funded by National Foundation for Science and Technology Development (NAFOSTED) Grant Number 103.01-2024.06. M.N.P.N acknowledges helpful discussions with Nguyen Van Long Thanh on the FALQON method.

## DATA AVAILABILITY

The data that support the findings of this article are openly available [40].

---

[1] N. Abdu, T. Tewelde, N. Jabir, S. Idrisnur, and E. H. Tesfamariam, Evaluation of potential drug-drug interactions and its determinants among outpatient prescriptions in six community chain pharmacies in asmara, eritrea: a cross-sectional study, *Scientific Reports* **15**, 33403 (2025).

[2] L. Li, J. Baker, R. Quirk, D. Deidun, M. Moran, A. A. Salem, N. Aryal, B. A. Van Dort, W. Y. Zheng, A. Hargreaves, P. Doherty, S. N. Hilmer, R. O. Day, J. I. Westbrook, and M. T. Baysari, Drug-drug interactions and actual harm to hospitalized patients: A multicentre study examining the prevalence pre- and post-electronic medication system implementation, *Drug Safety* **47**, 557 (2024).

[3] W. Y. Zheng, L. C. Richardson, L. Li, R. O. Day, J. I. Westbrook, and M. T. Baysari, Drug-drug interactions and their harmful effects in hospitalised patients: a systematic review and meta-analysis, *European Journal of Clinical Pharmacology* **74**, 15 (2018).

[4] C. Bucă, A. Farcaş, I. Cazacu, D. Leucuta, A. Achimas-Cadariu, C. Mogosan, and M. Bojita, How many potential drug&#x2013;drug interactions cause adverse drug reactions in hospitalized patients?, *European Journal of Internal Medicine* **24**, 27 (2013).

[5] J. Novak, A. Goldberg, K. Dharmarajan, A. Amini, R. J. Maggiore, C. J. Presley, and G. Nightingale, Polypharmacy in older adults with cancer undergoing radiotherapy: A review, *Journal of Geriatric Oncology* **13**, 778 (2022).

[6] A. Schmitz, C. Reichardt, J. Gierth, M. Richter, F. Mrosk, M. Alfertshofer, L. Knoedler, C. Doll, F. Hausmann, M. Lee, B. Kleikamp, C. Rendenbach, M. Heiland, and S. Koerdt, Retrospective analysis of multimorbidity, polypharmacy, and drug interactions on postoperative outcomes in oral squamous cell carcinoma patients, *Clinical Oral Investigations* **29**, 517 (2025).

[7] R. M. Alhumaidi, G. A. Bamagous, S. M. Alsanosi, H. S. Alqashqari, R. S. Qadhi, Y. Z. Alhindi, N. Ayoub, and A. H. Falemban, Risk of polypharmacy and its outcome in terms of drug interaction in an elderly population: A retrospective cross-sectional study, *Journal of Clinical Medicine* **12**, 10.3390/jcm12123960 (2023).

[8] M. R. Mohamed, S. G. Mohile, K. M. Juba, H. Awad, M. Wells, K. P. Loh, M. Flannery, E. Culakova, R. G. Tylock, and E. E. Ramsdale, Association of polypharmacy and potential drug-drug interactions with adverse treatment outcomes in older adults with advanced cancer, *Cancer* **129**, 1096 (2023),

https://acsjournals.onlinelibrary.wiley.com/doi/pdf/10.1002/[22]

[9] S. Ballestri, E. Romagnoli, D. Arioli, V. Coluccio, A. Marrazzo, A. Athanasiou, M. Di Girolamo, C. Cappi, M. Marietta, and M. Capitelli, Risk and management of bleeding complications with direct oral anticoagulants in patients with atrial fibrillation and venous thromboembolism: a narrative review, *Advances in Therapy* **40**, 41 (2023).

[10] J. Donzé, N. Rodondi, G. Waeber, J. Cornuz, and D. Aujesky, Major bleeding risk in anticoagulated patients receiving concomitant antiplatelet therapy: A prospective study, *Thrombosis Research* **131**, 502 (2013).

[11] S. Miernik, A. Matusiewicz, and M. Olesińska, Drug-induced myopathies: A comprehensive review and update, *Biomedicines* **12**, 10.3390/biomedicines12050987 (2024).

[12] L. Janssen, N. A. E. Allard, C. G. J. Saris, J. Keijer, M. T. E. Hopman, and S. Timmers, Muscle toxicity of drugs: When drugs turn physiology into pathophysiology, *Physiological Reviews* **100**, 633 (2020), pMID: 31751166, https://doi.org/10.1152/physrev.00002.2019.

[13] C. R. Dormuth, B. R. Hemmelgarn, J. M. Patterson, M. T. James, G. F. Teare, C. B. Raymond, J.-P. Lafrance, A. Levy, A. X. Garg, and P. Ernst, Use of high potency statins and rates of admission for acute kidney injury: multicenter, retrospective observational analysis of administrative databases, *BMJ* **346**, 10.1136/bmj.f880 (2013), https://www.bmjjournals.org/content/346/bmj.f880.full.pdf.

[14] D. Duarte and N. Vale, Evaluation of synergism in drug combinations and reference models for future orientations in oncology, *Current Research in Pharmacology and Drug Discovery* **3**, 100116 (2022).

[15] S. K. Singh, A. Mohammed, O. A. Alghamdi, and S. M. Husain, Chapter 12 - new approaches for targeting drug resistance through drug combination, in *Combination Therapy Against Multidrug Resistance*, edited by M. Y. Wani and A. Ahmad (Academic Press, 2020) pp. 221–246.

[16] Z. A. Shyr, Y.-S. Cheng, D. C. Lo, and W. Zheng, Drug combination therapy for emerging viral diseases, *Drug Discovery Today* **26**, 2367 (2021).

[17] L. Calzetta, C. Page, M. G. Matera, M. Cazzola, and P. Rogliani, Drug-drug interactions and synergy: From pharmacological models to clinical application, *Pharmacological Reviews* **76**, 1159 (2024).

[18] P. Vanessa, T. Nina, J. J. M., W. Brian, and K. F. C., Combinatorial approaches to the prevention and treatment of hiv-1 infection, *Antimicrobial Agents and Chemotherapy* **55**, 1831 (2011).

[19] R. B. Mokhtari, T. S. Homayouni, N. Baluch, E. Morgatskaya, S. Kumar, B. Das, and H. Yeger, Combination therapy in combating cancer, *Oncotarget* **8**, 38022 (2017).

[20] R. J. Worthington and C. Melander, Combination approaches to combat multidrug-resistant bacteria, *Trends in Biotechnology* **31**, 177 (2013), special Issue: Celebrating 30 years of biotechnology.

[21] S. Akinbolade, D. Coughlan, R. Fairbairn, G. McConkey, H. Powell, D. Ogunbayo, and D. Craig, Combination therapies for covid-19: An overview of the clinical trials landscape, *British Journal of Clinical Pharmacology* **88**, 1590 (2022), https://bpspubs.onlinelibrary.wiley.com/doi/pdf/10.1111/bcp.15089

[22] T. Babrowski, L. Chen, R. T. Eastman, Z. Itkin, P. Shinn, C. Z. Chen, H. Guo, W. Zheng, S. Michael, A. Simeonov, M. D. Hall, A. V. Zakharov, and E. N. Muratov, Synergistic and antagonistic drug combinations against sars-cov-2, *Molecular Therapy* **29**, 873 (2021).

[23] G. Li, R. Hilgenfeld, R. Whitley, and E. De Clercq, Therapeutic strategies for covid-19: progress and lessons learned, *Nature Reviews Drug Discovery* **22**, 449 (2023).

[24] Y. Wang, Z. Yang, and Q. Yao, Accurate and interpretable drug-drug interaction prediction enabled by knowledge subgraph learning, *Communications Medicine* **4**, 59 (2024).

[25] S. Wang, H. Yuan, Z. Hong, X.-g. Chen, and X. Yang, Path-based graph neural network for drug synergy prediction and interpretation, *Journal of Chemical Information and Modeling* 10.1021/acs.jcim.5c02569 (2025).

[26] J. Y. Ryu, H. U. Kim, and S. Y. Lee, Deep learning improves prediction of drug-drug and drug-food interactions, *Proceedings of the National Academy of Sciences* **115**, E4304 (2018), https://www.pnas.org/doi/pdf/10.1073/pnas.1803294115.

[27] L. Fillinger, S. Walter, M. Ley, K. Keska-Izworska, L. G. Dehkordi, K. Kratochwill, and P. Perco, Computational modeling approaches and regulatory pathways for drug combinations, *Drug Discovery Today* **30**, 104345 (2025).

[28] H. Luo, W. Yin, J. Wang, G. Zhang, W. Liang, J. Luo, and C. Yan, Drug-drug interactions prediction based on deep learning and knowledge graph: A review, *iScience* **27**, 109148 (2024).

[29] M. Zitnik, M. Agrawal, and J. Leskovec, Modeling polypharmacy side effects with graph convolutional networks, *Bioinformatics* **34**, i457 (2018).

[30] J. Chen, A. Lin, A. Jiang, C. Qi, Z. Liu, Q. Cheng, S. Yuan, and P. Luo, Computational frameworks transform antagonism to synergy in optimizing combination therapies, *npj Digital Medicine* **8**, 44 (2025).

[31] F. Glover, G. Kochenberger, and Y. Du, A tutorial on formulating and using qubo models (2019), arXiv:1811.11538 [cs.DS].

[32] L. Bittel and M. Kliesch, Training variational quantum algorithms is np-hard, *Phys. Rev. Lett.* **127**, 120502 (2021).

[33] E. Farhi, J. Goldstone, and S. Gutmann, A quantum approximate optimization algorithm (2014), arXiv:1411.4028 [quant-ph].

[34] J. R. McClean, S. Boixo, V. N. Smelyanskiy, R. Babbush, and H. Neven, Barren plateaus in quantum neural network training landscapes, *Nature Communications* **9**, 4812 (2018).

[35] A. B. Magann, K. M. Rudinger, M. D. Grace, and M. Sarovar, Feedback-based quantum optimization, *Phys. Rev. Lett.* **129**, 250502 (2022).

[36] T. N. V. Long, L. N. Tran, and L. B. Ho, Imaginary-time-enhanced feedback-based quantum algorithms for unstructured optimization (2025), arXiv:2512.13044 [quant-ph].

[37] T.-C. Chou, Theoretical basis, experimental design, and computerized simulation of synergism and antagonism in drug combination studies, *Pharmacological Reviews* **58**, 621 (2006).

[38] L. Rahmah, S. O. Abarikwu, A. G. Arero, M. Essouma, A. T. Jibril, A. Fal, R. Flisiak, R. Makuku, L. Marquez, K. Mohamed, L. Ndow, D. Zarkebska-Michaluk, and P. Rezaei, Oral antiviral treatments for

covid-19: opportunities and challenges, *Pharmacol. Rep.* **74**, 1255 (2022).

[39] D. K. Brady, A. R. Gurijala, L. Huang, A. A. Hussain, A. L. Lingan, O. G. Pembridge, B. A. Ratangee, T. T. Sealy, K. T. Vallone, and T. P. Clements, A guide to COVID-19 antiviral therapeutics: a summary and perspective of the antiviral weapons against SARS-CoV-2 infection, *FEBS J.* **291**, 1632 (2024).

[40] M. N. P. Nhi, L. N. Tran, and L. B. Ho, Supporting data for drug-drug interaction optimization using the feedback-based quantum control algorithms (2026), <https://github.com/echkon/ddi>, <https://github.com/echkon/ddi> (2026).